*J. Fluid Mech.* (1983), *vol.* 129, *pp.* 443–453
*Printed in Great Britain*



# The evolution of Tollmien–Schlichting waves near a leading edge. Part 2. Numerical determination of amplitudes

By M. E. GOLDSTEIN, P. M. SOCKOL AND J. SANZ
National Aeronautics and Space Administration, Lewis Research Center, Cleveland, Ohio 44135

(Received 19 August 1982 and in revised form 17 November 1982)

It was shown in Part 1 that the amplitude of the spatially growing Tollmien–Schlichting wave generated by a time-harmonic free-stream disturbance is related to the coefficient multiplying the lowest-order Lam & Rott asymptotic eigensolution of the unsteady boundary-layer equation. In this part we use a numerical solution of the unsteady boundary-layer equation to determine that coefficient for the case of a uniformly pulsating stream.

## 1. Introduction

In Part 1 of this paper (Goldstein 1983) it was shown that, in the limit $\epsilon \equiv (\nu\omega/U_\infty^2)^{\frac{1}{2}} \to 0$, the unsteady motion induced in a laminar boundary layer by a small-amplitude free-stream disturbance of frequency $\omega$ and inverse spatial scale $O(\omega/U_\infty)$, where $U_\infty$ is the upstream mean flow velocity and $\nu$ is the kinematic viscosity, is governed by the linearized unsteady boundary-layer equation in the region near the leading edge where the normalized streamwise distance from that edge $x \equiv \omega x^+/U_\infty$ is $O(1)$. The solution to this equation asymptotically approaches a Stokes shear-wave-type solution plus a linear combination of asymptotic eigensolutions as $x \to \infty$. The Stokes-type solution is independent of the behaviour of the full unsteady boundary-layer solution, which describes the motions in the upstream region where $x \leqslant O(1)$. The solution in this latter region affects the asymptotic solution only through the coefficients in the linear combination of asymptotic eigensolutions, which are in fact completely determined by this upstream solution, and, since the latter is proportional to the amplitude of the free-stream disturbance, the coefficients of the asymptotic eigensolutions also have this property.

Only the asymptotic eigensolutions of Lam & Rott (1960) were studied. They were shown to be non-uniformly valid in $x$ when considered as solutions to the full Navier–Stokes equations – the unsteady motion in the downstream region, where $x_1 \equiv \epsilon^2 x = O(1)$, being governed by the Orr–Sommerfeld equation and not the unsteady boundary-layer equation, which determines the asymptotic eigensolutions. However, we showed that the Tollmien–Schlichting wave solutions of the former equation match, in the matched-asymptotic-expansion sense, onto the Lam & Rott asymptotic eigensolutions and are consequently the natural continuations of these solutions into the downstream region. The Tollmien–Schlichting waves are given by equation (6.1) of part 1 in high-Reynolds-number slowly varying approximation appropriate to the $\epsilon \to 0$ limit that is of interest here. This equation can be written as

$$u_1 = \epsilon^{-2\gamma} C_1 A_0(x_1) \frac{\partial \gamma}{\partial \eta} \exp\left[\frac{i}{\epsilon}\int_0^x \kappa(x_1, \epsilon)\, dx\right], \tag{1.1}$$

where we have introduced the new slowly varying amplitude function

$$A_0(x_1) \equiv A(x_1)\,(2x_1)^{-\frac{1}{2}}.$$

and multiplied the result by the $O(1)$ constant $C_1$. Explicit formulas were given for all terms in this equation except the constant $C_1$. But, when $A$ is normalized in the manner implied by (6.2) of part 1, $C_1$ is the same as the constant that multiplies the corresponding asymptotic Lam & Rott (1960) eigensolution of the unsteady boundary-layer equation and must therefore be determined by 'patching' the numerical solution of this equation onto its large-$x$ asymptotic expansion.

Ackerberg & Phillips (1972), who studied the case of a uniformly pulsating stream, attempted to do this by fitting the numerically calculated fluctuating displacement thickness to the asymptotic expansion of this quantity, which, as we already indicated, consists of a Stokes shear-wave-type expansion plus a linear combination of asymptotic eigensolutions. They determined the numerical constants in this combination by requiring that the asymptotic solution agree with the numerical solution at certain preselected points. They used only the Lam & Rott eigensolutions and therefore implicitly assumed that these eigenfunctions are, in some sense, complete. This cannot, of course, be proved, but even if completeness is assumed their procedure is subject to a number of criticisms, which were pointed out to the first author by a referee of part 1.

First, as indicated in part 1, Ackerberg & Phillips' formulas for the asymptotic eigenfunctions are in error owing to the omission of a factor of $x^r$. Secondly, their choice of the eigenfunctions to be included was somewhat *ad hoc* in that they omitted the lowest-order asymptotic eigenfunction, which, incidentally, is the one of primary interest in the present context. Thirdly, and possibly most seriously, they obtained different values for the constants that multiply the asymptotic eigenfunctions depending on whether they matched the in-phase or out-of-phase component of the displacement thickness.

One purpose of the present paper is therefore to re-do their calculation in a way that overcomes these objections. Since, as we indicated, our interest here is in the coefficient of the lowest-order asymptotic eigenfunction, which is the one that exhibits the most rapid decay, but which is also the one that matches onto the only Tollmien–Schlichting wave that eventually exhibits spatial growth, the success of our procedure depends on the asymptotic expansion being numerically significant at relatively small values of $x$. The numerical evidence indicates that this is the case when the optimal approximation for the Stokes-layer expansion is used.

But even when all this is done the procedure is, at best, uncertain and it is highly desirable to check the coefficient of the lowest-order asymptotic eigenfunction by using a completely independent method to determine its value. To this end, we use the result, established by Lam & Rott (1960), that the solution of the unsteady boundary-layer equation is an analytic function of the independent variable $x$, when $x$ is extended into the complex plane. The numerical solution of the unsteady boundary-layer equation can therefore be analytically continued into the region of the complex $x$-plane where the lowest-order asymptotic eigensolution (which is subdominant for real $x$) is dominant. It is then quite easy to find the coefficient of this eigenfunction, but one must be sure that no Stokes discontinuities are introduced in the process. This turns out to be the case in the present analysis, as demonstrated in §2 and as evidenced by the fact that *the coefficient obtained by the analytic continuation procedure is quite close to the coefficient obtained from the patching procedure described above.*

These calculations involve the numerical solution of the unsteady boundary-layer equation. Our algorithm, which is simpler than the one used by Ackerberg & Phillips (1972) and which we found to be quite accurate, is described in appendix A.

Brown & Stewartson (1973*a*) found an infinite set of eigensolutions of the unsteady boundary-layer equation that achieve their peak values just outside the steady boundary layer and are therefore, on the face of it, quite different from those of Lam & Rott (1960). However, we show in §3 that the Lam & Rott eigenfunctions are non-uniformly valid with increasing order and we argue that the Brown & Stewartson eigenfunctions may be obtainable by re-expanding (for large $x$) an appropriate sum of the Lam & Rott eigenfunctions provided that the latter are first rendered uniformly valid.

In fact, the Brown & Stewartson (1973*a*) expansion requires that $(\ln \frac{1}{3}x)^{\frac{1}{2}}$ be much greater than unity rather than the much weaker condition $x \gg 1$ required for the validity of the Lam & Rott eigenfunctions. We therefore expect that the former will only become valid much further downstream than the Lam & Rott eigenfunctions.

On the other hand, the higher-order Lam & Rott eigenfunctions, which become increasingly poor asymptotic approximations as their order increases, become more important relative to the lower-order ones as the streamwise distance increases, since their decay rate decreases with increasing order. We therefore expect that the Lam & Rott eigenfunctions may be sort of intermediate asymptotics that best describe the numerical solution at moderately large values of $x$.

The present work completes the solution of the 'receptivity' problem described in §1 of part 1. A completely numerical solution was previously given by Murdock (1980), but he had to impose an artificial upstream boundary condition at a finite distance from the leading edge. Related analytical studies were carried out by Rogler & Reshotko (1977) and by Tam (1981).

## 2. Numerical determination of coefficients

In this section we estimate the coefficients of the lower-order Lam & Rott (1960) asymptotic eigenfunctions for an infinitely thin flat plate in a uniformly oscillating stream (with velocity $U_\infty + u_\infty e^{-i\omega t}$ where $u_\infty = \text{constant}$); first by modifying the Ackerberg & Phillips (1972) procedure to eliminate the faults listed in §1, and secondly by analytically continuing the numerical solution into the complex plane.

To carry out the first procedure, we extend the Stokes-layer expansion one order higher than Ackerberg & Phillips (1972). This is easily accomplished by continuing their procedure. We therefore merely give the final result for the fluctuating displacement thickness $\delta^* e^{-i\omega t}$, which, in the notation of part 1, is given by

$$\begin{aligned}\delta^* &= \epsilon^3 \int_0^\infty \left( u_\infty (2x)^{\frac{1}{2}} - \frac{\partial \psi_0}{\partial \eta} \right) d\eta \\ &= \epsilon^3 \lim_{\eta \to \infty} ((2x)^{\frac{1}{2}} u_\infty \eta - \psi_0). \end{aligned} \tag{2.1}$$

The contribution $\delta^*_{\mathrm{St}}$ from the Stokes-layer expansion is given by

$$\frac{\delta^*_{\mathrm{St}}}{\epsilon^3 u_\infty (2x)^{\frac{1}{2}}} = \frac{1+i}{2x^{\frac{1}{2}}} - \frac{i\beta}{2x} - \frac{13}{32}\frac{U_0'}{x^2} + i\frac{39}{64}\frac{U_0'}{x^3} + \frac{4051}{2048}\frac{(1-i)\,U_0'^2}{x^{\frac{7}{2}}} + O(x^{-4}), \tag{2.2}$$

where $\beta = \lim_{\eta \to \infty} (\eta F' - F) = 1{\cdot}21678$, $U_0'$ is given by (3.8) of part 1, and it should

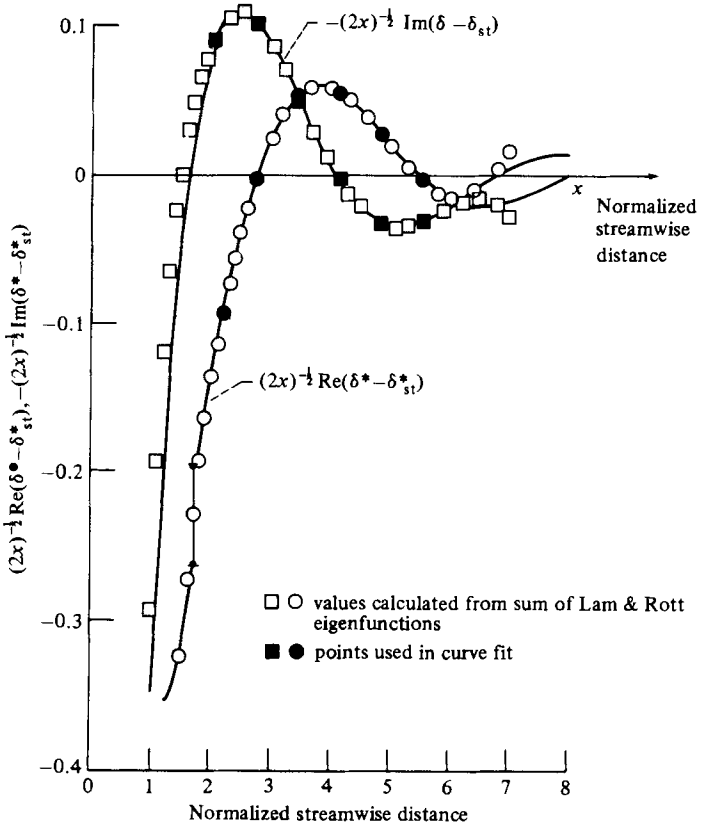


FIGURE 1. Difference between fluctuating displacement thickness amplitude calculated from numerical solution and that calculated from asymptotic Stokes-type solution.

be recalled that our result is the complex conjugate of that of Ackerberg & Phillips (1972),† since our time dependence enters through the factor $e^{-i\omega t}$.

As pointed out by Bender & Orszag (1978, p. 94), the 'optimal asymptotic approximation' is obtained by finding the smallest term in the expansion and then omitting it along with all higher-order terms. This means that we should neglect all $O(x^{-2})$ terms in (2.2) when $1 < x < 1{\cdot}73$, but retain the $x^{-2}$ term and neglect all $O(x^{-3})$ when $1{\cdot}73 < x < 2{\cdot}32$. The error is small enough when $x > 2{\cdot}32$ so that we need not be overly concerned with the optimal approximation in this region.

The unsteady boundary-layer equation was solved numerically by using *the procedure* described in appendix A. It is quite similar to, but somewhat simpler than, the one used by Ackerberg & Phillips (1972). We used the result to calculate $\delta^*/\epsilon^3 u_\infty (2x)^{\frac{1}{2}}$, and in figure 1 we plot the real and imaginary parts of the difference between this result and that predicted by the Stokes-layer expansion (2.2). The discontinuity at $x \approx 1{\cdot}73$ is due to the fact that we used the optimal approximation for $\delta^*_{\mathrm{St}}/\epsilon^3 u_\infty (2x)^{\frac{1}{2}}$.

Following Ackerberg & Phillips, we fitted these curves numerically at six equally spaced points by using a linear combination of the Lam & Rott asymptotic eigenfunctions. However, we worked with the corrected eigenfunctions of part 1 and

† There is a factor of $\sqrt{2}$ missing in the $O(\alpha^5)$ term of Ackerberg & Phillips' equation (3.39). Also the last member of their equation (3.13) should be omitted and the 5 on the right-hand side of their equation (3.14) should be replaced by a 4.

| Order $n$ | Eigenvalue $\zeta_n$ | Exponent $\tau$ |
|---|---|---|
| 1 | −1·0188 | −0·69213 |
| 2 | −3·2482 | −0·27037 |
| 3 | −4·8201 | 0·71653 |
| 4 | −6·1633 | 2·2674 |
| 5 | −7·3722 | 4·3823 |
| 6 | −8·4885 | 7·0613 |
| 7 | −9·5354 | 10·304 |
| 8 | −10·538 | 14·111 |
| 9 | −11·475 | 18·482 |
| 10 | −12·385 | 23·416 |

TABLE 1. Exponents for coefficients of first 10 Lam & Rott asymptotic eigenfunctions

| Order $n$ | Coefficients | |
|---|---|---|
| | Re $C_n/u_\infty$ | Im $C_n/u_\infty$ |
| 1 | −0·42041 | 0·81804 |
| 2 | 1·15536 | 0·18063 |
| 3 | −0·24266 | 0·13681 |
| 4 | 0·00811 | −0·01426 |
| 5 | −0·00002 | 0·00020 |
| 6 | −0·00000 | −0·00000 |

TABLE 2. Coefficients of asymptotic eigenfunctions obtained from curve fit shown in figure 1

| Order $n$ | Coefficients | |
|---|---|---|
| | Re $C_n/u_\infty$ | Im $C_n/u_\infty$ |
| 1 | −0·45266 | 0·82661 |
| 2 | 1·03376 | 0·34942 |
| 3 | −0·22173 | 0·08619 |
| 4 | 0·00732 | −0·00986 |
| 5 | −0·00002 | 0·00011 |

TABLE 3. Coefficients of asymptotic eigenfunctions obtained from curve fit of displacement thickness difference using only first 5 eigenfunctions

retained the first six eigenfunctions in the expansion. Moreover, the same complex constants were used to fit both the real and imaginary parts. Thus, as can be seen from (2.14), (3.7*a*) and (3.15) of part 1, we fitted the curves by

$$\frac{\delta^* - \delta^*_{\mathrm{St}}}{\epsilon^3 u_\infty (2x)^{\frac{1}{2}}} \approx \sum_{n=1} \frac{C_n}{u_\infty}\left(1 + \frac{iU_0'}{\lambda_n (2x)^{\frac{1}{2}}}\right) x^{\tau_n} \exp\left[-\frac{\lambda_n (2x)^{\frac{3}{2}}}{3U_0'}\right],$$

where $\lambda_n = \lambda$ is given by (3.9) and (3.13) of part 1, and the exponents $\tau_n = \tau$ of the corrected eigenfunctions are given by (3.16) of part 1. This latter formula is simplified in appendix B, where it is shown that $\tau$ is a real quantity. The values of $\tau$ corresponding to the first 10 eigenfunctions are listed in table 1 along with the associated roots of (3.13) of part 1.

The solid circles in figure 1 represent the equally spaced points used for the curve

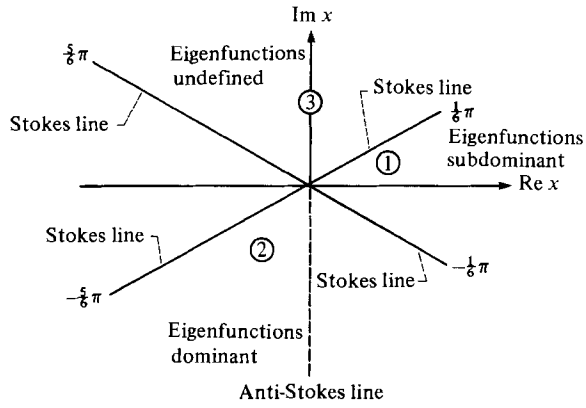


FIGURE 2. Stokes lines for asymptotic eigenfunctions of Lam & Rott.

fit. The resulting values of the coefficients are listed in table 2. It can be seen that they decrease rapidly with increasing order.

We attempted fitting the curve with more than six eigenfunctions, but this led to a matrix that was too ill-conditioned to invert. This is due to the fact that the contributions from the successively higher-order eigenfunctions tend to become more important at larger values of $x$.

However, we were able to fit the curves with the first five eigenfunctions. The fit was not quite as good as when six eigenfunctions were used, but the resulting coefficients, which are listed in table 3, were not substantially changed.

The open circles in figure 1 are calculated from the six-term eigenfunction expansion. We believe the agreement is encouraging, but it could probably be improved by retaining higher-order terms in the Lam & Rott functions. This can be done by extending the analysis of appendix A of part 1. In fact, the next highest-order terms can easily be calculated once the constant $K$ is found. But this involves evaluating some complicated integrals and we have not attempted to do that. However, we did introduce the next-highest-order term with $K$, which is primarily determined by the solvability condition for the next-order solution, set equal to zero. This improved the fit of the imaginary part of $\delta^*/u_\infty\,\epsilon^3(2x)^{\frac{1}{2}}$ at both small and large values of $x$. The fit at large values of $x$ could probably have been further improved if we had been able to use more of the higher-order asymptotic eigenfunctions, but as we indicated in §1, they are probably quite inaccurate.

The Stokes lines for the asymptotic eigenfunctions are shown in figure 2. The eigenfunctions are expotentially small in sector ①, and the lowest-order eigenfunction decays most rapidly there. However, it exhibits the most rapid growth in sector ②, where the asymptotic eigenfunctions are exponentially large. The eigenfunctions do not exist in sector ③.

In sector ① the asymptotic eigenfunctions first appear on the Stokes line $\arg x = \frac{1}{6}\pi$ along which they undergo their most rapid decay.† They then contribute to the

† Dingle (1973, pp. 5–19) points out that Stokes discontinuities must occur in an asymptotic expansion if that expansion is to comply with the variations of the continuous function it represents, but these discontinuities, which are manifested by the sudden appearance of a new asymptotic series, arise in the most efficient and least disruptive way imaginable: they occur along the Stokes ray ($\arg x = \frac{1}{6}\pi$ in our case) where the new series is at an absolute minimum relative to the continuing series (the Stokes shear-wave solutions in our case).

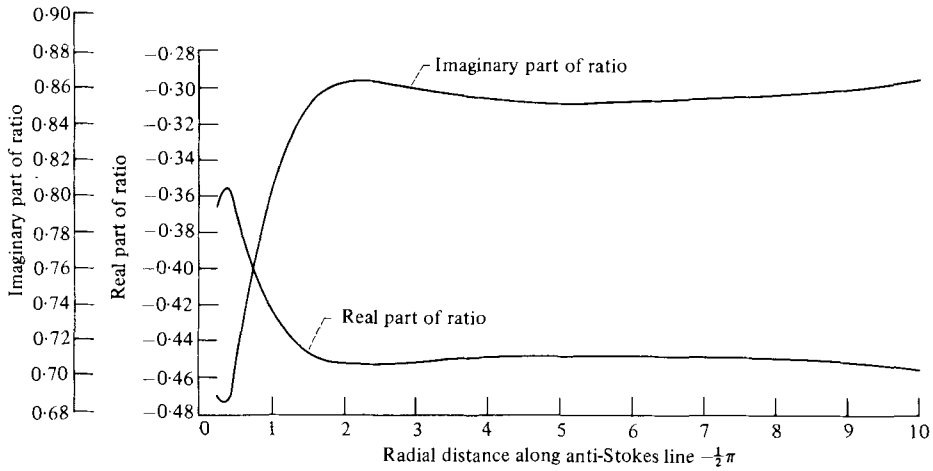


FIGURE 3. Ratio of numerical solution to $u_\infty \times$ lowest-order Lam & Rott asymptotic eigenfunction as $x$ varies along anti-Stokes line $-\frac{1}{2}\pi$.

solution with the same numerical coefficients throughout this sector and the portion of sector ② lying between the Stokes line $\arg x = -\frac{1}{6}\pi$ and the anti-Stokes line $\arg x = -\frac{1}{2}\pi$ (Dingle 1973, p. 12). Brown & Stewartson (1973*b*) demonstrated analytically that the complete solution of a simplified asymptotic model of the unsteady boundary layer equation behaves in this precise fashion.

When $x$ is in section ②, the numerical solution should behave like the lowest-order asymptotic eigensolution at sufficiently large values of $|x|$. The ratio of these two solutions should, therefore, become independent of $x$ as $|x|$ increases along any radial line in this sector. In figure 3 this ratio is plotted as a function of $|x|$ as $x$ varies along a radial line slightly to the right of anti-Stokes line $\arg x = -\frac{1}{2}\pi$ where the exponential growth rate of the eigenfunction is maximum. It can be seen that the ratio changes rapidly for $|x| < 1$ but is fairly constant for $1 < |x| < 8$, even though the numerical and asymptotic solutions individually increase by several orders of magnitude when $|x|$ increases by one unit at the larger values of $|x|$. The variations that occur when $|x| > 8$ are due to the fact that our numerical solution has not converged in this region.

From figure 3 we estimate that the coefficient of the lowest-order asymptotic eigenfunctions is roughly equal to $-0{\cdot}45 + 0{\cdot}855i$. Approximately the same value was obtained when the integration was carried out along several other radial lines in sector ②. Notice that this number is quite close to the value listed in table 2, which was obtained from the curve fit along the positive real axis – indicating that the coefficient of the lowest-order asymptotic eigensolution does not change as the solution is analytically continued from the real axis into sector ②.

## 3. Validity of Lam & Rott eigenfunctions and connection with Brown & Stewartson eigenfunctions

As we saw in part 1, the Lam & Rott eigenfunctions, say $\psi_n^{\mathrm{LR}}(x)$, were constructed by matching an inner wall-layer solution, which applies when $\sigma \equiv \eta(2x)^{\frac{1}{2}}$ is $O(1)$ and $x \gg 1$, with an outer solution, which applies when $\eta = O(1)$.

The inner expansion is expressed in terms of Airy functions whose arguments $\zeta_{\mathrm{b}}$ are given by (3.11) of part 1. Hence, as the order $n$ of the eigenfunctions increases, the asymptotic behaviour of the inner solution is achieved at larger and larger values

of $\sigma$, that is, at fixed $x$ the size of the inner region increases with increasing order. The value of $x$ must then be increased in order to reduce the size of this region relative to that of the steady boundary layer. The higher-order asymptotic eigenfunctions therefore become accurate approximations at much larger values of $x$ than do the lower-order eigenfunctions. This means that the limit as $x \to \infty$ and the limit as $n \to \infty$ cannot be interchanged.

Since the asymptotic expansions used to construct the eigenfunctions are associated with the limit as $x \to \infty$ with $n$ held fixed while the sum

$$S(x) = \sum_{n=1}^{\infty} C_n \psi_n^{\mathrm{LR}}(x) \tag{3.1}$$

involves the limit as $n \to \infty$ with $x$ held fixed, we cannot hope to evaluate this series by using the Lam & Rott asymptotic expansions for the eigenfunctions $\psi_n^{\mathrm{LR}}$, *unless the value of this series is primarily determined by its lowest-order terms.*

The results of §2 show that the coefficients $C_n$ decrease very rapidly with increasing $n$, but, as we have seen, the lower-order asymptotic eigenfunctions decay more rapidly with $x$ than the higher-order eigenfunctions. Hence the sum (3.1) should provide the best approximation to the numerical solution at intermediate values of $x$ when the asymptotic approximations to $\psi_n^{\mathrm{LR}}$ are used. We certainly cannot take the limit $\lim_{x\to\infty} S(x)$ unless a uniformly valid approximation of the $\psi_n^{\mathrm{LR}}$ is first inserted into (3.1).

As we indicated in §1, Brown & Stewartson (1973*a*) obtained a different set of asymptotic eigenfunctions, which apply when $(\ln \frac{1}{3}x)^{\frac{1}{2}} \gg 1$ and are therefore only valid much further downstream than the Lam & Rott eigenfunctions, which apply when $x \gg 1$. It is therefore not unreasonable to expect that, *conceptually*, each Brown & Stewartson (1973*a*) eigenfunction can be expressed as a large-$x$ asymptotic expansion of a sum of the form (3.1) in which a uniformly valid approximation for the $\psi_n^{\mathrm{LR}}$ is used. The Brown & Stewartson (1973*a*) functions would then be determined by the 'infinite tail' of the series (3.1), which is precisely where the non-uniformly valid Lam & Rott expansions break down. Now we have seen that this breakdown occurs because the higher-order asymptotic eigensolutions tend to move away from the wall as their order increases. It is therefore not surprising that Brown & Stewartson's functions are centred at the outer edge of the steady boundary layer. They will probably match onto the continuous spectrum of the Orr–Sommerfeld equation – but this is only speculation at this point.

## 4. Concluding remarks

In part 1 we matched the spatially growing Tollmien–Schlichting wave solution of the Orr–Sommerfeld onto a certain asymptotic eigensolution of the unsteady boundary-layer equation and thereby related the amplitude of this wave to that of the eigensolution. In this part we used a numerical solution of the unsteady boundary-layer equation to relate the amplitude of the asymptotic eigensolution, and consequently of the Tollmien–Schlichting wave, to that of the imposed free-stream disturbance for the special case of a uniformly pulsating stream. The ideas of this paper can be extended to other more complex bodies and free-stream oscillations.

## Appendix A. Numerical solution of the unsteady boundary-layer equation

In this appendix we present a finite-difference method for solving the unsteady boundary-layer equation (3.2) of part 1. Our procedure is similar to, but somewhat simpler than, the one used by Ackerberg & Phillips (1972).

Introducing the new variable

$$G \equiv \psi_0/(2x)^{\frac{1}{2}}, \tag{A 1}$$

(3.2) can be rewritten as the pair

$$G_\eta - W = 0, \tag{A 2}$$

$$W_{\eta\eta} + FW_\eta + F''G - 2x\left[F'W_x - F''G_x - \frac{du_\infty}{dx} - i(W-u_\infty)\right] = 0. \tag{A 3}$$

Following Ackerberg & Phillips (1972), we introduce the mesh points $(x_n, \eta_j)$, for $x \geqslant 0$, $0 \leqslant \eta \leqslant \eta_J$, and use the notation

$$x_1 = 0, \quad x_{n+1} = x_n + k \quad (n = 1, 2, 3, \ldots), \tag{A 4}$$

$$\eta_1 = 0, \quad \eta_{j+1} = \eta_j + h \quad (j = 1, 2, 3, \ldots, J-1). \tag{A 5}$$

Only two $x$-stations $(n, n+1)$ have to be considered at once, and, again following Ackerberg & Phillips, we denote values at the old station $x_n$ by overbars. Then, for any dependent variable $\phi$, we use the abbreviated notation

$$\phi \equiv \phi(x_{n+1}, \eta_j), \quad \bar{\phi} \equiv \phi(x_n, \eta_j), \tag{A 6}$$

$$\hat{\phi} \equiv \tfrac{1}{2}(\phi + \bar{\phi}). \tag{A 7}$$

Introducing the difference operators

$$\delta_\eta^2 f_j \equiv f_{j+1} - 2f_j - f_{j-1},$$

$$\mu_\eta \delta_\eta f_j \equiv \tfrac{1}{2}(f_{j+1} - f_{j-1}),$$

(A 3) can be approximated by

$$-\frac{1}{h^2}(\delta_\eta^2 + hF_j\mu_\eta\delta_\eta)\hat{W}_j - F_j''\hat{G}_j + \frac{2}{k}\hat{x}[2F_j'(\hat{W}_j - \bar{W}_j)$$
$$-2F_j''(\hat{G}_j - \bar{G}_j) - ik(\hat{W}_j - \hat{u}_\infty) - 2(\hat{u}_\infty - \bar{u}_\infty)] = 0 + O(h^2, k^2). \tag{A 8}$$

Using centred differences, approximating (A 2) at the point $(\hat{x}, \eta_{j+\frac{1}{2}})$ and collecting terms in (A 8), we obtain, for $j = 1, 2, \ldots, J$,

$$\hat{G}_j = \hat{G}_{j-1} + \tfrac{1}{2}h(\hat{W}_j + \hat{W}_{j-1}), \tag{A 9}$$

$$-A_j\hat{W}_{j-1} + B_j\hat{W}_j - C_j\hat{W}_{j+1} - D_j\hat{G}_j = E_j, \tag{A 10}$$

where we have put

$$\delta \equiv \frac{k}{h^2}, \quad \theta \equiv -ik\hat{x}, \tag{A 11}$$

$$A_j \equiv \delta(1 - \tfrac{1}{2}hF_j), \quad C_j \equiv \delta(1 + \tfrac{1}{2}hF_j), \tag{A 12}$$

$$B_j \equiv 2(\delta + \theta + 2\hat{x}F_j'), \tag{A 13}$$

$$D_j \equiv F_j''(k + 4\hat{x}), \tag{A 14}$$

$$E_j \equiv 4\hat{x}(F_j'\bar{W}_j - F_j''\bar{G}_j) + 2\theta\hat{u}_\infty + 4x(\hat{u}_\infty - \bar{u}_\infty). \tag{A 15}$$

The appropriate initial condition is discussed by Ackerberg & Phillips (1972). It requires that we put

$$G_j = \tfrac{1}{2}(\eta_j F_j' + F_j) \quad (x_1 = 0, j = 1, 2, \ldots, J). \tag{A 16}$$

Starting from this condition, we can march downstream and solve (A 9) and (A 10) at $x = x_{n+1}$ for $\hat{G}_j$ and $\hat{W}_j$, $j = 1, 2, \ldots, J$, using their known values at the previous station $x = x_n$. The boundary conditions given by (3.3) and (3.5) of part 1 require that the solution satisfy

$$\hat{G}_1 = \hat{W}_1 = 0, \tag{A 17}$$

$$\hat{W}_J = \hat{u}_\infty. \tag{A 18}$$

Once this solution is found, we can use (A 7) to calculate $\phi$, which is the new value of $\bar{\phi}$ for the calculation at the next $x$-step.

In order to solve (A 9) and (A 10) at $x = x_n$ we introduce the *Ansatz*

$$\hat{W}_j = R_j + S_j \hat{W}_{j-1} + T_j \hat{G}_{j-1} \tag{A 19}$$

and use it along with (A 9) to eliminate $W_{j+1}, G_j$ in (A 10). This yields

$$-A_j \hat{W}_{j-1} + B_j \hat{W}_j - C_j(R_{j+1} + S_{j+1} \hat{W}_j) - (D_j + C_j T_{j+1})[G_{j-1} + \tfrac{1}{2}h(\hat{W}_j + \hat{W}_{j-1})] = E_j.$$

Comparing this with (A 19) shows that the Ansatz will hold if we put

$$\beta_j \equiv D_j + C_j T_{j+1}, \tag{A 20}$$

$$\alpha_j \equiv B_j - C_j S_{j+1} - \tfrac{1}{2}h\beta_j, \tag{A 21}$$

$$R_j = \frac{E_j + C_j R_{j+1}}{\alpha_j}, \tag{A 22}$$

$$S_j = \frac{A_j + \frac{1}{2}h\beta_j}{\alpha_j}, \tag{A 23}$$

$$T_j = \frac{\beta_j}{\alpha_j}. \tag{A 24}$$

It follows that we can calculate $\hat{W}_j$ and $\hat{G}_j$ from the following algorithm. First, we satisfy (A 18) by setting $R_J = \hat{u}_\infty$ and $S_J = T_J = 0$. Then we use (A 20)–(A 24) to calculate successively $R_j, S_j$ and $T_j$ beginning at $j = J-1$ and ending at $j = 2$.

Once these quantities are known, we can use (A 17) to calculate $\hat{G}_1$ and $\hat{W}_1$ and then use (A 9) and (A 19) to calculate successively $\hat{G}_j$ and $\hat{W}_j$ beginning at $j = 2$ and ending at $j = J-1$.

## Appendix B. Simplification of formula for $\tau$

Using (3.7*b*) of part 1 to eliminate $g_0$ and $g_0'$ in the denominator of (3.16) of Part 1 and integrating both the numerator and denominator of the result by parts yields

$$\frac{-\tau U_0'}{\int_0^\infty w\, d\sigma} = \frac{\int_0^\infty \left(\sigma^2 g_0''' - 2g_0' + \frac{\lambda\sigma^4}{12} g_0'' - \lambda\sigma^2 g_0\right) w\, d\sigma}{4\int_0^\infty w^2 \sigma\, d\sigma}.$$

Using the equation preceding (A 7) of part 1 to eliminate $g_0'''$ and then using (A 16)

to eliminate $(\lambda\sigma+i)\,w$ in the result yields

$$\frac{-\tau U_0'}{\int_0^\infty w\,d\sigma} = \frac{\int_0^\infty \left[\sigma^2 g_0' w'' + w\left(\frac{\lambda\sigma^2}{12} g_0'' - 2g_0'\right)\right] d\sigma}{4\int_0^\infty w^2\sigma\,d\sigma} = \frac{\int_0^\infty w\left[(\sigma^2 g_0')'' + \frac{\lambda\sigma^4}{12} g_0'' - 2g_0'\right] d\sigma}{4\int_0^\infty w^2\sigma\,d\sigma}. \tag{B 1}$$

Differentiating the second line of (3.7) of part 1 shows that

$$g_0'' = \frac{U_0' w}{\int_0^\infty w\,d\sigma}.$$

Using this to eliminate $g_0''$ in (B 1) yields

$$\tau = -\frac{\int_0^\infty \left(4w\sigma + \sigma^2 w' + \frac{\lambda\sigma^4}{12} w\right) w\,d\sigma}{4\int_0^\infty w^2\sigma\,d\sigma}.$$

Hence upon integrating by parts we obtain

$$\tau = -\frac{1}{4}\left[3 + \frac{\lambda}{12}\frac{\int_0^\infty w^2\sigma^4\,d\sigma}{\int_0^\infty w^2\sigma\,d\sigma}\right].$$

Using (3.10), (3.11) and (3.14) of part 1, introducing the new variable of integration

$$z = \frac{e^{\frac{1}{4}i\pi}}{\rho_n^{\frac{1}{3}}}\sigma$$

in place of $\sigma$, and deforming the new integration contours to lie along the real axis, we obtain

$$\tau = -\frac{1}{4}\left\{3 - \frac{1}{12}\frac{\int_0^\infty z^4[\mathrm{Ai}\,(z-\rho_n)]^2\,dz}{\int_0^\infty [z\,\mathrm{Ai}\,(z-\rho_n)]^2\,dz}\right\}, \tag{B 2}$$

which shows that $\tau$ is real.

## REFERENCES


Ackerberg, R. C. & Phillips, J. H. 1972 *J. Fluid Mech.* **51**, 137.

Bender, C. M. & Orszag, S. A. 1978 *Advanced Mathematical Methods for Scientists and Engineers.* McGraw-Hill.

Brown, S. N. & Stewartson, K. 1973*a* *Proc. Camb. Phil. Soc.* **73**, 493.

Brown, S. N. & Stewartson, K. 1973*b* *Proc. Camb. Phil. Soc.* **73**, 505.

Dingle, R. B. 1973 *Asymptotic Expansions: Their Derivation and Interpretation.* Academic.

Goldstein, M. E. 1983 *J. Fluid Mech.* **127**, 59.

Lam, S. H. & Rott, N. 1960 Theory of linearized time-dependent boundary layers. *Cornell Univ. Grad. School of Aero. Engng Rep.* AFOSR TN-60-1100.

Murdock, J. W. 1980 *Proc. R. Soc. Lond.* **A372**, 517.

Rogler, H. L. & Reshotko, E. 1977 In *Proc. Intl Symp. on Modern Developments in Fluid Dynamics* (ed. J. Rom), p. 150. SIAM.

Tam, C. K. W. 1981 *J. Fluid Mech.* **109**, 483.